

Contents lists available at ScienceDirect

Petroleum Science

journal homepage: www.keaipublishing.com/en/journals/petroleum-science



Original Paper

Investigation of gravity influence on EOR and CO₂ geological storage based on pore-scale simulation



Yong-Mao Hao ^{a, b, *}, Gui-Cheng Wu ^{a, b}, Zong-Fa Li ^c, Zhong-Hui Wu ^{a, b}, Yong-Quan Sun ^d, Ran Liu ^d, Xing-Xing Li ^{a, b}, Bo-Xin Pang ^{a, b}, Nan Li ^{a, b}

- ^a Key Laboratory of Unconventional Oil & Gas Development (China University of Petroleum (East China)), Ministry of Education, Qingdao, 266580, Shandong, China
- ^b School of Petroleum Engineering, China University of Petroleum (East China), Qingdao, 266580, Shandong, China
- ^c School of Petroleum Engineering, Yangtze University, Wuhan, 430100, Hubei, China
- d Dongsheng Jinggong Petroleum Development Group Co., Ltd, Shengli Oilfield Company, SINOPEC, Dongying, 257001, Shandong, China

ARTICLE INFO

Article history: Received 24 July 2023 Received in revised form 24 November 2023 Accepted 28 November 2023 Available online 7 December 2023

Edited by Yan-Hua Sun

Keywords: Gravity Flow simulation CO₂—oil mixing Enhanced oil recovery (EOR) Geological storage

ABSTRACT

Gravity assistance is a critical factor influencing CO₂—oil mixing and miscible flow during EOR and CO₂ geological storage. Based on the Navier—Stokes equation, component mass conservation equation, and fluid property—composition relationship, a mathematical model for pore-scale CO₂ injection in oil-saturated porous media was developed in this study. The model can reflect the effects of gravity assistance, component diffusion, fluid density variation, and velocity change on EOR and CO₂ storage. For non-homogeneous porous media, the gravity influence and large density difference help to minimize the velocity difference between the main flow path and the surrounding area, thus improving the oil recovery and CO₂ storage. Large CO₂ injection angles and oil—CO₂ density differences can increase the oil recovery by 22.6% and 4.2%, respectively, and increase CO₂ storage by 37.9% and 4.7%, respectively. Component diffusion facilitates the transportation of the oil components from the low-velocity region to the main flow path, thereby reducing the oil/CO₂ concentration difference within the porous media. Component diffusion can increase oil recovery and CO₂ storage by 5.7% and 6.9%, respectively. In addition, combined with the component diffusion, a low CO₂ injection rate creates a more uniform spatial distribution of the oil/CO₂ component, resulting in increases of 9.5% oil recovery and 15.7% CO₂ storage, respectively. This study provides theoretical support for improving the geological CO₂ storage and EOR processes.

© 2023 The Authors, Publishing services by Elsevier B.V. on behalf of KeAi Communications Co. Ltd. This is an open access article under the CC BY-NC-ND license (http://creativecommons.org/licenses/by-nc-nd/4.0/).

1. Introduction

The CO₂ injection in oil reservoirs is a promising method for improving crude oil recovery (Cheng et al., 2017; Gong et al., 2020; Wang et al., 2021). In addition, CO₂ flooding in oil reservoirs is the most economical and feasible approach to achieving large-scale CO₂ storage (Tao et al., 2009; Zhang, 2013; Liu and Rui, 2022).

Indoor experiments have shown that gravity-assisted gas flooding can significantly improve oil recovery and CO₂ storage effect. Yang et al. (2020) established a two-dimensional visual

E-mail address: haoyongmao@163.com (Y.-M. Hao).

model of a seam-hole and performed top-injection nitrogen replacement experiments. The experimental results showed that the secondary gas top formed by gravity partitioning was key in improving oil recovery from seam-hole-type reservoirs (Yang et al., 2020). Long et al. (2021) arranged the core samples in different angles and performed gravity-assisted air flooding experiments. They found that with the angle increased from 0° to 90°, the oil recovery increased from 37.2% to 57.5%, and 54.6% of the oil was recovered owing to the assisting effect of gravity (Long et al., 2021). Han et al. (2016) conducted experiments on CO₂ near-miscible flooding under vertical and horizontal core conditions. The results showed that injecting CO₂ from the bottom decreased the recovery by 7.8% and the CO₂ storage amount by approximately half (Han et al., 2016). Adel et al. (2018) investigated the effect of gravity on recovery at different injection pressures and found that the

^{*} Corresponding author. Key Laboratory of Unconventional Oil & Gas Development (China University of Petroleum (East China)), Ministry of Education, Qingdao, 266580, Shandong, China.

effect of gravity on recovery decreased with increasing injection pressure. When the injection pressure was 11.6 MPa, the gravityassisted effect improved oil recovery by approximately 59.7%. When the injection pressure was 15 MPa, CO₂ mixed with oil, and the gravity-assisted effect increased recovery by 6.4% (Adel et al., 2018). Peng et al. (2020) established a three-dimensional largescale physical model and conducted top-gas, bottom-water, and conventional water injection experiments. The top-air injection recovered 40.0% of the oil, which was higher than those of the bottom-water and conventional water injection scenarios (Peng et al., 2020). Huang et al. (2021) conducted gravity-assisted airflooding experiments and found that crude oil production within the pre-gas scramble stage accounted for 80% of the entire gasflooding process under gravity-assisted action (Huang et al., 2021). Previous studies have shown that gravity-assisted action is essential in improving the recovery of the reservoir gas flooding. The recovery of the reservoir gas flooding significantly increases under gravity-assisted action.

In order to study the flow mechanism of fluids within porous media more directly, the researchers simulated the fluid flow process using pore-scale numerical simulation method, which can describe the velocity, composition, etc. of the fluid at each spatial location (Yang et al., 2013; Kitao et al., 2021; Sepehri and Siavashi, 2022). Wang et al. (2022a) analyzed the migration pattern and distribution of injected CO2 through pore-scale numerical simulation method. The modeling results showed that CO2 migrated mainly along the high-porosity and large-pore-size layers, leaving a large area of low-porosity and small-pore-size regions not displaced (Wang et al., 2022a). Li et al. (2023a) established a numerical model of CO₂ miscible flooding. The microscopic seepage characteristics of interphase mass transfer in CO₂ miscible flooding were analyzed by multiphysics field coupling simulations at the twodimensional pore scale. The research showed that after injection into the model, CO₂ preferentially diffuses into the large pore space and forms a miscible area with crude oil through interphase mass transfer, and the miscible area expands continuously and is pushed to the outlet by the high CO₂ concentration area (Li et al., 2023a). Behnoud et al. (2023) focused on pore-scale near-miscible CO₂—oil displacement. The results indicated that interface is moved into the by-passed oil due to low interfacial tension in the near-miscible region. Moreover, behind the front ahead of the main flow stream, the CO₂ phase can significantly displace almost all the bypassed oil in normal pores and effectively decrease the large amounts in small pores (Behnoud et al., 2023). Liu and Song (2015) conducted an investigation of CO2 flooding, adopting pore-scale reconstructed model to analyze the complex interplay of displacing and displaced fluid in a porous media (Liu and Song, 2015). Yan et al. (2022) developed a single-phase, two-component flow model by coupling the Navier-Stokes equation and mass transfer equation to reveal the potential mechanisms of the miscibility and displacement of crude oil and hydrocarbon gases. The simulation results demonstrated that the residual oil content is lower at low gas injection velocity than that at high gas injection velocity due to the better miscibility of fluids (Yan et al., 2022). Wang et al. (2022b) investigated the diffusion of CO2 components during CO2 throughput using the lattice Boltzmann method. They focused on simple pore structures and did not assess the effects of changes in the physical properties of the fluid (Wang et al., 2022b). Kong et al. (2020) performed pore-scale simulations of a non-miscible gravityassisted gas flooding using CFD. The simulation results showed that under the effect of gravity, the injected gas could overcome the capillary force of the narrow pore throats and displace the oil in those throats to improve oil recovery (Kong et al., 2020). Song et al. (2023) performed two-phase flow simulations to simulate the CO₂ flooding process based on the phase-field method. A multipleparameter analysis was performed to investigate the effects of capillary number, viscosity ratio, wettability, density, gravity, interfacial tension, and absolute permeability on the two-phase fluid flow characteristics. The results indicated that with a low capillary number, the flooding process of the injected CO2 was mainly controlled by the capillary force and gravity (Song et al., 2023). In the previous work, there are relatively few studies of pore-scale numerical simulation considering gravity. In addition, in the previous pore-scale numerical simulation model, the diffusive mass transfer of components and their resulting changes in fluid physical properties during CO₂ flooding are ignored, which reduces the simulation accuracy. Therefore, in this study, a mathematical model reflecting the effect of gravity on CO2 miscible flooding in porous media was established, considering the effects of the CO₂ injection angle, injection velocity, component diffusion coefficient, and CO₂—oil density difference in the CO₂ flooding process. The aim of this study was to reveal the mechanisms of gravity influence on CO₂ geological storage. Based on the spatial distribution of the fluid velocity and the component concentration distribution in the porous medium, the effects of the injection angle, injection velocity, diffusion, and fluid density difference on the oil recovery and CO₂ geological storage were analyzed.

2. Mathematical model of miscible oil— CO_2 flow considering gravity assistance

In the CO_2 flooding process, the spatial distribution of fluid flow and component diffusion within the porous medium are nonuniform owing to the complex pore—throat structure. This results in significant differences in the fluid density at various locations in the porous medium. With the aid of gravity, the lower density fluid flows from the top region of the porous medium, whereas the higher density fluid tends to flow from the bottom of the porous medium.

In this mathematical model, the flow process of an oil-CO₂ miscible fluid within the porous medium obeys the law of momentum conservation, and is expressed by the Navier-Stokes equation (Eq. (1)). In this study, the variation in fluid momentum is influenced by the pressure, viscous forces, and gravity. It is assumed that CO₂ and oil are in a single-contact miscible state; that is, CO₂ can achieve a miscible state with oil at the first contact. Therefore, in the proposed model, the effect of interfacial tension is ignored in the Navier-Stokes equation. During the CO₂ miscible flooding, the fluid composition and fluid density are not uniformly distributed spatially at each location, and the fluid flow always obeys the mass conservation law for compressible fluids (Eq. (2)). In Eqs. (3) and (4), the fluid density is the product of the weighted CO₂ density and oil density, with the weight being the molar concentration of the CO₂ and oil components. Under the miscible state, elevated temperatures and pressures do not cause further phase changes in the fluid and have a less important effect on the fluid properties compared with immiscible state (Zhang et al., 2020b; Xi et al., 2022). Under miscible state, the most important influencing factor is the fluid composition, which has been considered in the model (Soomro et al., 2023). Besides, considering that high temperature and pressure will greatly increase the difficulty of convergence and reduce the efficiency of calculation (Lauser et al., 2011; Sun et al., 2023). Therefore, only the influence of the most important factor (composition) on fluid properties is considered.

$$\rho \frac{\partial \mathbf{u}}{\partial t} + \rho(\mathbf{u} \cdot \nabla)\mathbf{u} = \nabla \cdot [-p\mathbf{I} + \mu(\nabla \mathbf{u} + (\nabla \mathbf{u})^{\top}) - \frac{2}{3}\mu(\nabla \cdot \mathbf{u})\mathbf{I}] + \rho \mathbf{g}$$
(1)

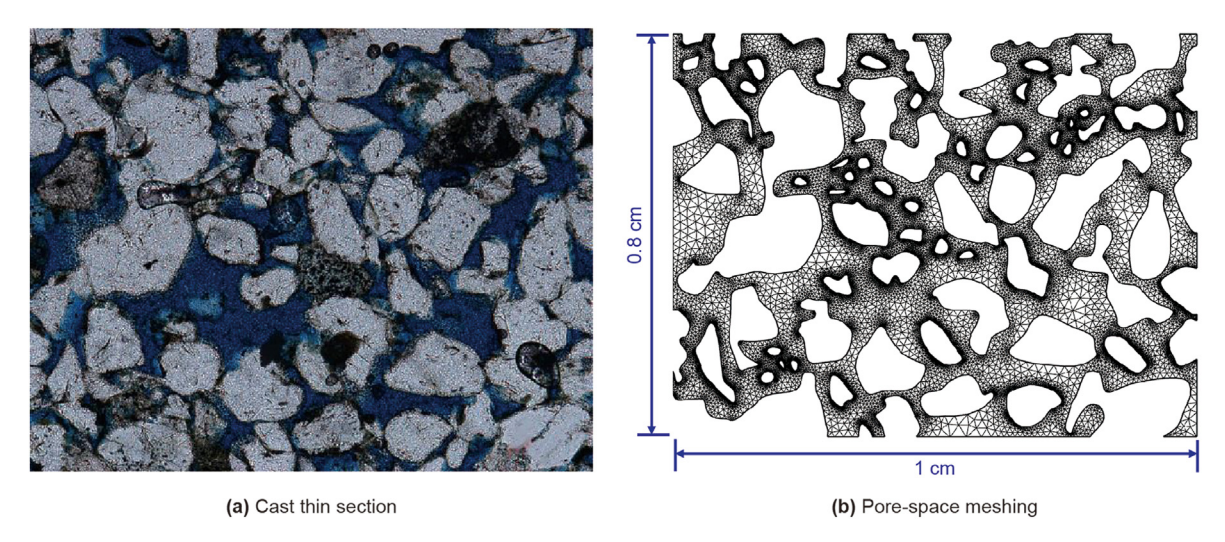


Fig. 1. Porous media: pore-throat structure and meshing.

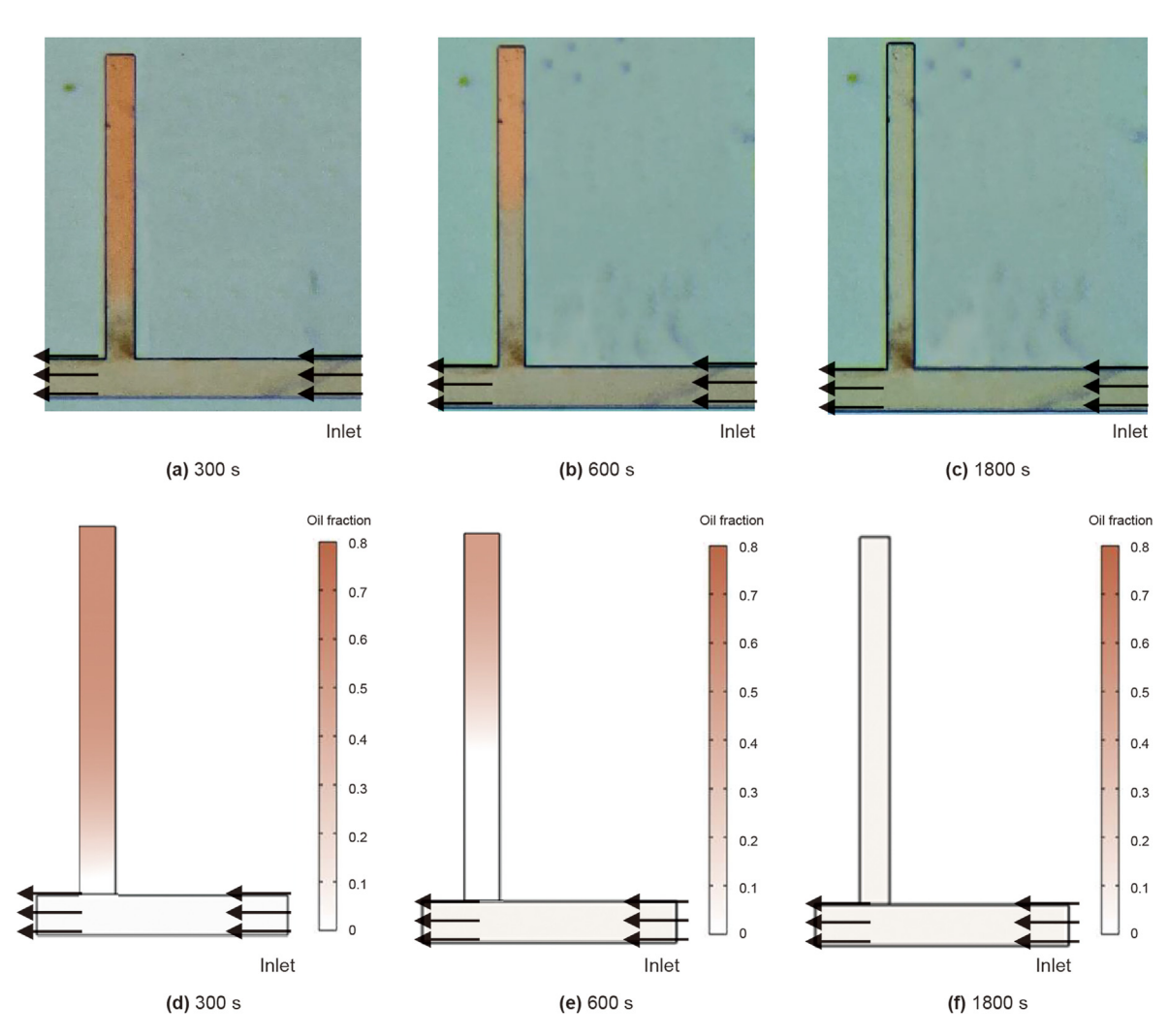


Fig. 2. Distribution of oil fractions between calculations of this study and experimental observations of Li et al. (2023b).

$$\frac{\partial \rho}{\partial t} + \nabla \cdot (\rho u) = 0 \tag{2}$$

$$\rho = x_{\text{CO}_2} \rho_{\text{CO}_2} + x_{\text{oil}} \rho_{\text{oil}} \tag{3}$$

$$x_{\text{CO}_2} + x_{\text{oil}} = 100\% \tag{4}$$

where ρ is the fluid density, kg/m³; u is the fluid velocity, m/s; t is the time, s; p is the fluid pressure, MPa; μ is the fluid viscosity, mPa s; I is the dimensionless identity matrix; g is the gravity acceleration of the fluid, m²/s; x_{CO_2} is the CO₂ mole fraction; and x_{oil} is the oil mole fraction.

At the porous medium inlet, the CO_2 injection velocity was 6×10^{-5} m/s (Eq. (5)), corresponding to a CO_2 -displacement leading-edge movement velocity of 5.18 m/d. The porous-medium outlet was maintained at a constant pressure of 50 MPa (Eq. (6)). At the start of the CO_2 flooding, the fluid in the porous medium was at rest (Eq. (7)), and the fluid pressure was 50 MPa (Eq. (8)).

$$u_{\text{inlet}} = 0.00006 \text{ m/s}$$
 (5)

$$p_{\text{outlet}} = 50 \text{ MP}$$
 (6)

$$u_{t=0} = 0 \text{ m/s}$$
 (7)

$$p_{t=0} = 50 \text{ MPa}$$
 (8)

In the CO_2 miscible flooding process, influenced by the complex pore throat structure, the distribution of the fluid flow velocity within the porous medium widely varies in space. The oil and CO_2 components are not uniformly distributed within the dead-end pores, and strong component diffusion occurs. Therefore, the variation in the amount of oil or CO_2 component at various locations within the porous medium is influenced by the fluid flow and oil or CO_2 component diffusion (Eq. (9)). In Eq. (9), the first term on the left is the CO_2 or oil component accumulation term, the second term is the CO_2 or oil component diffusion mass flux term, and the third term on the left is the CO_2 or oil component flow mass flux term

$$\rho \frac{\partial \omega_i}{\partial t} + \nabla \cdot J_i + \rho(u \cdot \nabla)\omega_i = 0 \tag{9}$$

where ω_i is the CO₂ or oil mass fraction of the fluid (Eq. (10)); J_i is the CO₂ or oil diffusive mass flux (Eq. (11)), kg/(m²/s).

$$\omega_i = \frac{x_i M_{ri}}{\sum\limits_{j=1}^{N} x_j M_{rj}} \tag{10}$$

$$J_i = \rho d \nabla \omega_i \tag{11}$$

where M_r is the CO₂ or oil relative molecular mass of the fluid; d is the diffusion coefficient, which is equal to 20×10^{-10} m²/s.

At the entrance of the porous media, the molar content of CO_2 in the fluid is 100% (Eqs. (12) and (13)). At the pore walls of the porous media, no diffusion of the oil and CO_2 components normal to the pore walls occurs (Eq. (14)). At the onset of the CO_2 flooding, the fluid in the porous media comprised only oil (Eqs. (15) and (16)). At the exit of the porous medium, the oil and CO_2 components flowed out from the porous medium according to the boundary conditions of Danckwerts (Eq. (14)). The sum of the mass fractions of the oil

and CO_2 components at each location within the porous medium is 100% (Eq. (17)).

$$\omega_{\text{inlet}}(\text{CO}_2) = 100\% \tag{12}$$

$$\omega_{\text{inlet}}(\text{oil}) = 0\%$$
 (13)

$$\mathbf{n} \cdot \mathbf{J}_i = \mathbf{0} \tag{14}$$

$$\omega_{t=0}(\mathsf{CO}_2) = 0\% \tag{15}$$

$$\omega_{t=0}(\text{oil}) = 100\% \tag{16}$$

$$\omega(\text{CO}_2) + \omega(\text{oil}) = 100\% \tag{17}$$

In this study, core samples were collected from the target reservoir, and core cast sheets were produced (Fig. 1(a)). Information of pore-throat structure was obtained from the cast sheet. The whole calculation domain structure has been automatically meshed and locally refined based on the free triangle mesh through the COMSOL multiphysics software package. The pore space within the porous media was discretized into 37,678 triangular meshes with a minimum mesh size of 2×10^{-3} cm (Fig. 1(b)). Some of the pore throats are relatively small. In order to calculate the results more accurately, the grids of small pores are denser, thus the small pores appear to be closed and unconnected. Actually, in the porous media of this study, all pores are connected.

The partial differential equations of the simulation model are discretized by finite element method embedded in COMSOL software, which has the advantage of solving problems with very complex combinations of factors, such as inhomogeneous material properties, arbitrary boundary conditions, complex geometries (Ye and Zhang, 2020; Sun et al., 2021). To avoid convergence problems

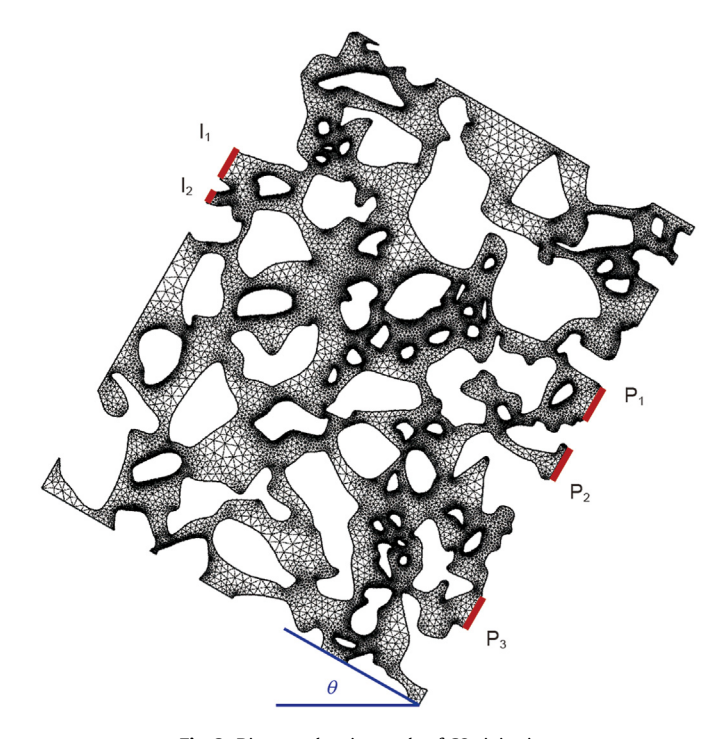


Fig. 3. Diagram showing angle of CO₂ injection.

Table 1 Pore and fluid characteristics.

Porous media size, cm		Minimum pore size, cm	Oil density, kg/m³	CO ₂ density, kg/m ³	Oil molecular weight, g/mol	CO ₂ molecular weight, g/mol	Oil viscosity, Pa s	CO ₂ viscosity, Pa s
Length	Width							
1.0	0.8	2×10^{-3}	720	320	126	44	1.5	0.05

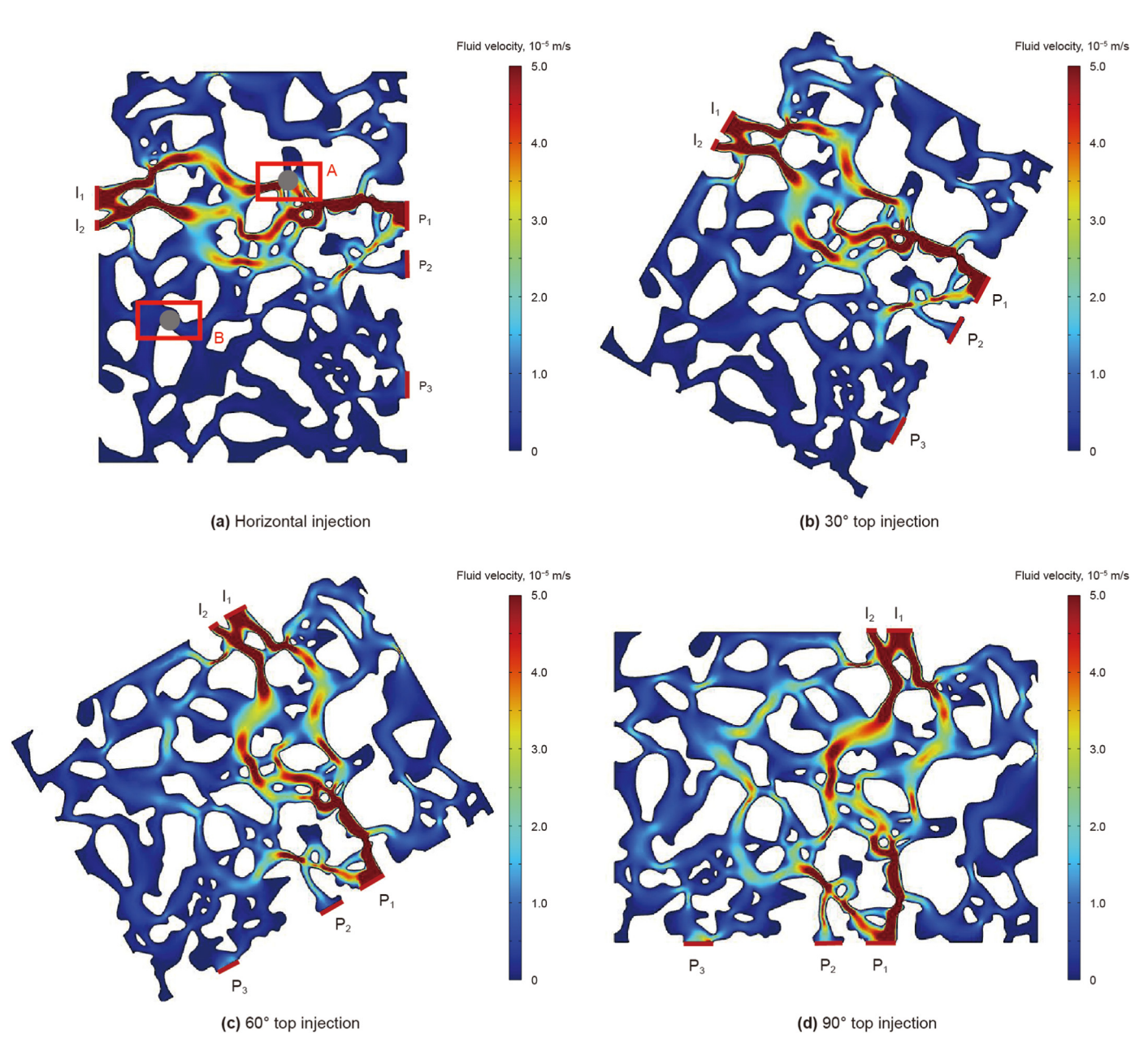


Fig. 4. Spatial distribution of fluid velocities at different injection angles after 800 s of CO₂ injection.

and slow convergence rate, the direct sparse linear system solver PARDISO embedded in COMSOL is applied to solve the model equations. The principle of PARDISO solver is to use symmetric matrices, shared memory parallel processing, and one-step inverse method for solving. It has the advantages of convenient use, strong robustness, and memory-saving, and is suitable for small problems, highly nonlinear, and multi physical field problems, etc. (Long et al., 2020; Zhang et al., 2020a).

In order to verify the accuracy of the model, the simulation of CO_2 miscible flooding within the dead-end pore space was carried out, and the simulation results was compared with the experimental observations in Li's research (Li et al., 2023b). The initial conditions, boundary conditions, and the fluid physical properties were referred to Li's study. The simulated results of oil component distribution in this study were in good agreement with the experimental results of Li et al. (2023b) (Fig. 2).

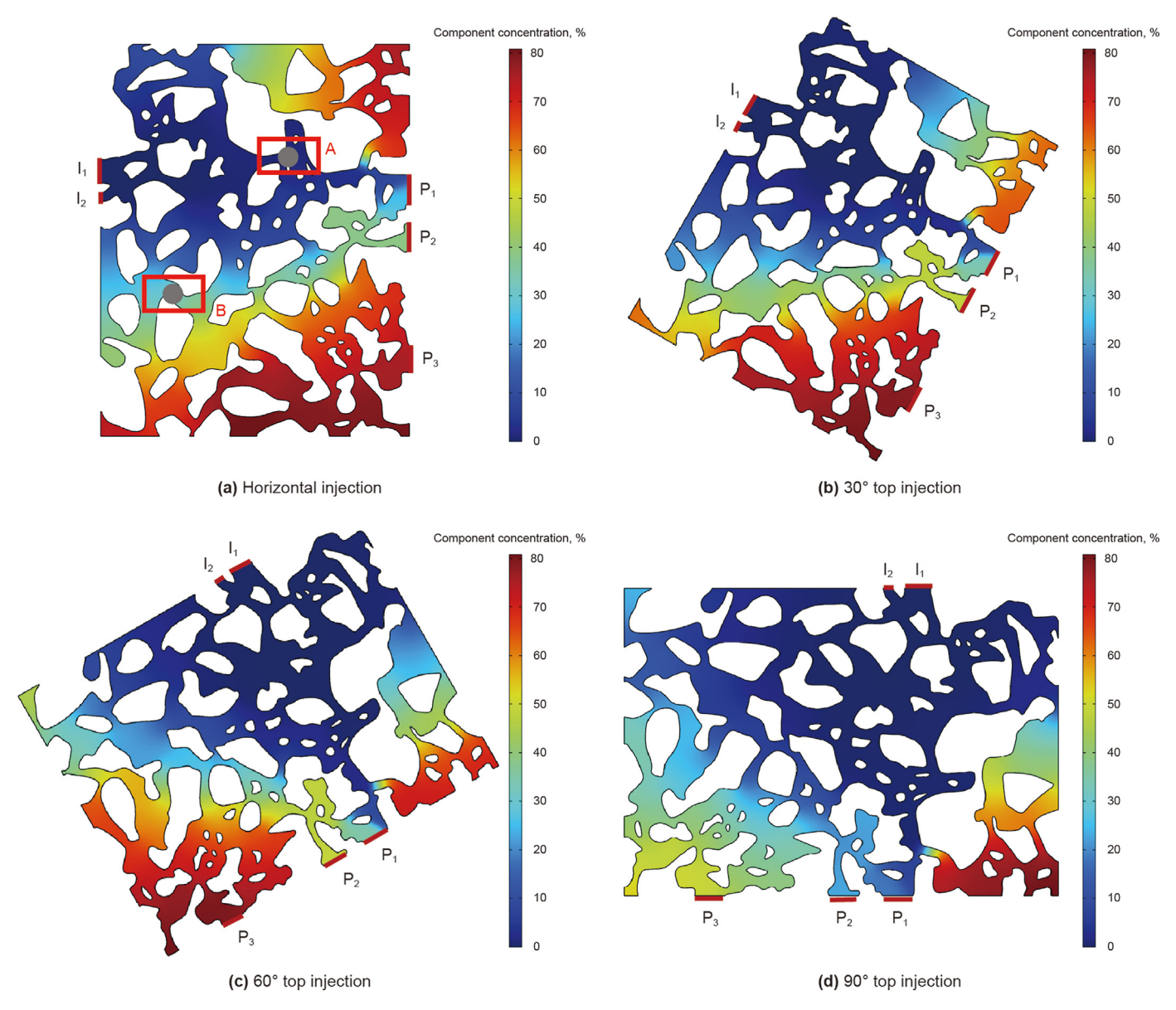


Fig. 5. Spatial distribution of component concentrations at different injection angles after 800 s of CO₂ injection.

Table 2Velocity, oil component concentration at each marker point in porous media, and breakthrough time.

Injection angle, °	Velocity, 10 ⁻⁵ m/s		Oil mole fraction at B, %	Breakthrough time, s
	Point A	Point B		
0	12.10	0.32	35	216
15	10.55	0.92	27	227
30	8.05	1.43	19	240
45	6.72	1.92	11	255
60	5.36	2.52	5	270
75	4.81	2.82	2	286
90	4.26	3.16	1	300

3. Results and discussion

3.1. Injection angle

The inclination angle of the reservoir significantly influences CO₂ flooding and storage. Some reservoirs use CO₂-assisted SAGD to

achieve CO_2 flooding and storage, in which CO_2 flows vertically from the top towards the production well (Wang et al., 2018; Beaton et al., 2022). The porous media was rotated by θ angles (0°, 30°, 60°, and 90°), and the CO_2 flooding and storage effects were simulated for different CO_2 injection angles using the proposed mathematical model. In this study, CO_2 injection was assumed

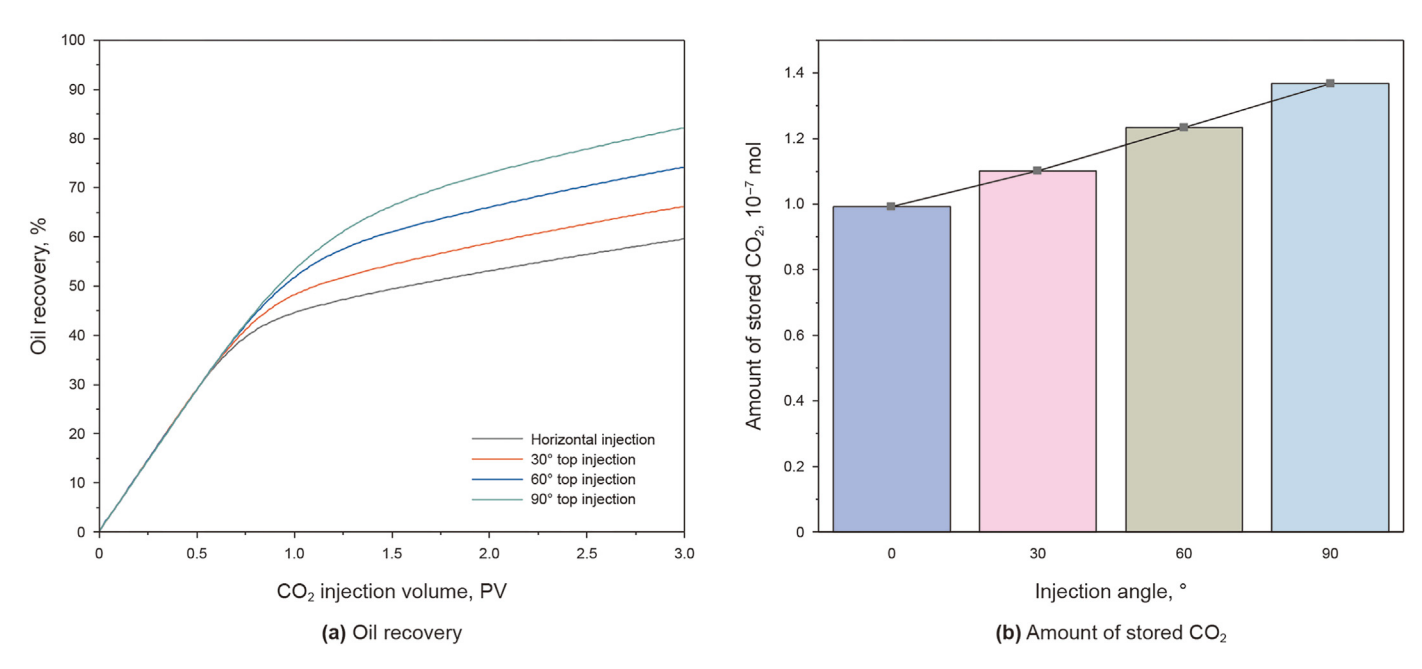


Fig. 6. Variations in oil recovery and CO₂ storage amount at different injection angles.

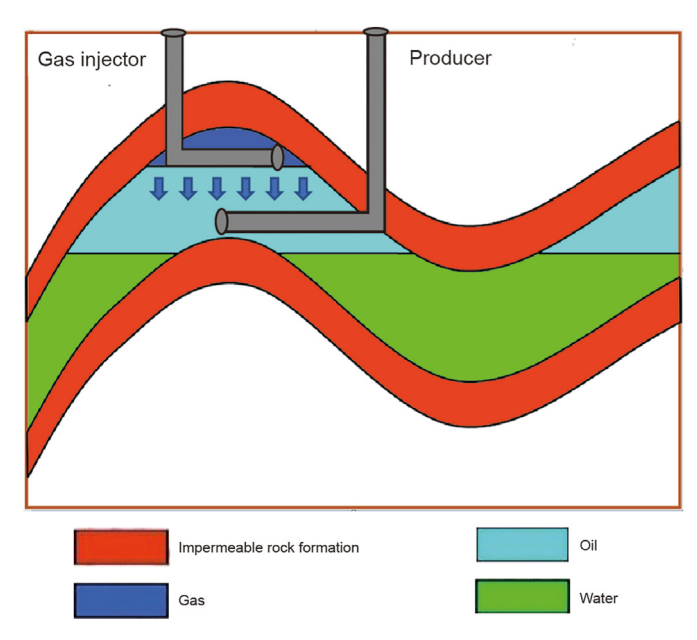


Fig. 7. CO₂ flooding process in the oil reservoirs with a gas cap.

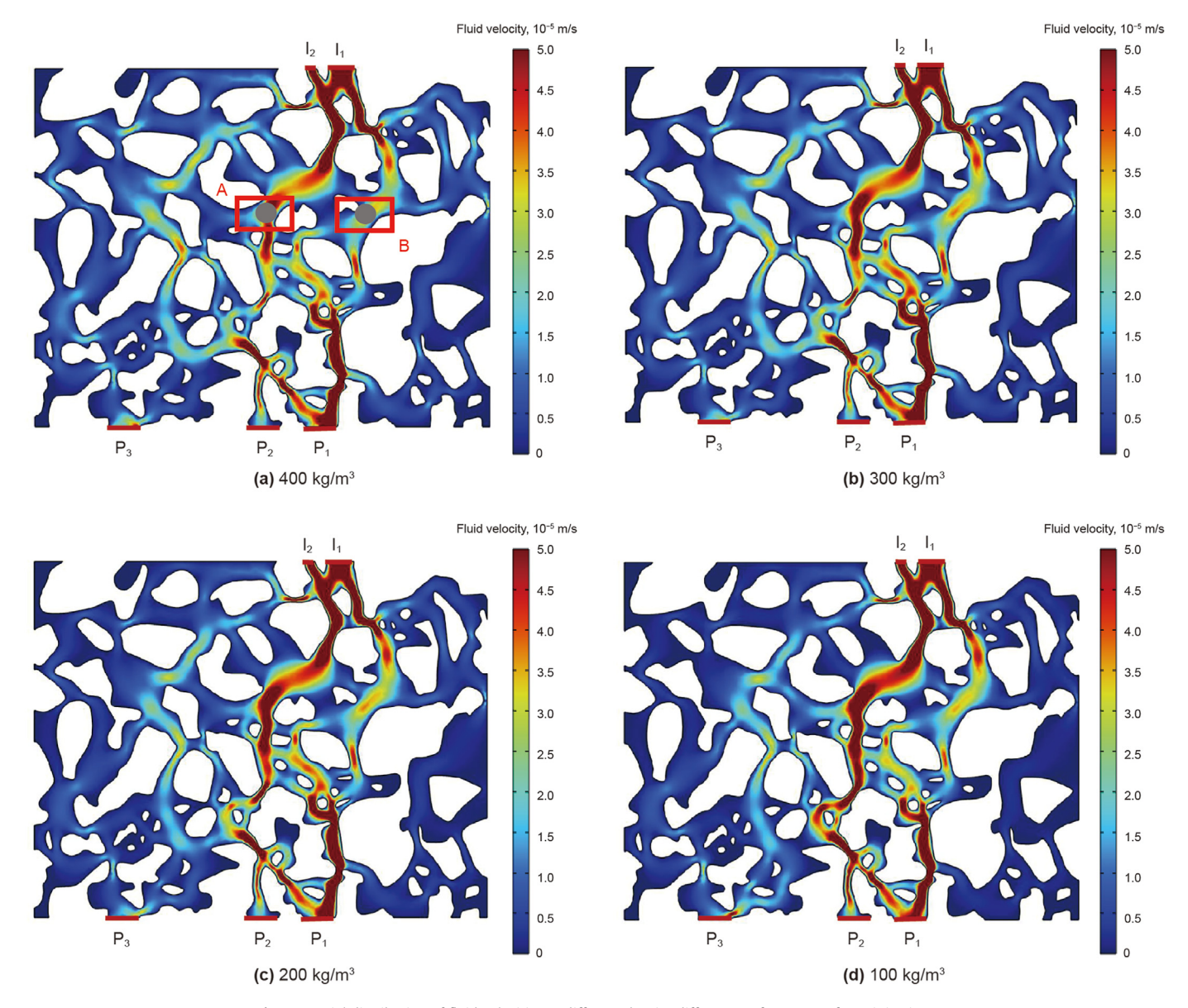
above the porous media (I_1 and I_2), crude oil production was adopted at the bottom (P_1 , P_2 , and P_3), and the boundary conditions were kept constant (Fig. 3).

The CO₂—oil density difference is 400 kg/m³ and the specific gravity of the injected oil is 0.72. CO₂ injection velocity is 6×10^{-5} m/s and component diffusion coefficient is 5.4×10^{-9} m²/s. The pore and fluid properties used in the model are shown in Table 1.

Based on the fluid velocity distribution within the porous medium, the fluid within the porous medium mainly flowed in the flow channel between the inlets (I_1 and I_2) and P_1 when CO_2 was injected in the horizontal direction (rotated by 0° , Fig. 4(a)). The

low fluid flow velocities at outlets P_2 and P_3 indicated that less fluid flowed out from P_2 and P_3 . Because the density of CO_2 is lower than that of crude oil, CO_2 gradually moves upward as it is transported. Therefore, the crude oil above the inlets (I_1 and I_2) was displaced better (Fig. 5(a)), with the molar fraction of the oil component at point A being 34% lower than that at point B. It should be mentioned that the spatial distribution of component concentrations used in this study is mole fraction, according to Eq. (10), the mole fraction and mass fraction are interconvertible. Therefore, the two factors describe similar spatial distribution of oil concentrations. In addition, as shown in Eq. (4), the sum of the mole fractions of CO_2 and oil is 100%. Therefore, the spatial distribution of CO_2 concentration can be indirectly represented by the distribution of component concentration of oil.

If the inlet is higher than the outlet, the CO₂ will have a downward displacement component during transportation to the outlet. In this study, the larger the angle of rotation of the porous medium, the larger the displacement component in the vertical direction during CO₂ transportation to the outlet. The longer the CO₂ transport distance in the vertical direction, the stronger the effect of the gravity-assisted CO2-oil density difference, the lower the fluid velocity along the flow path between I₁ and P₁, and the significantly higher the fluid velocity in the area around the main flow path (Fig. 4). Taking points A and B as examples (Fig. 4(a)), as the injection angle increased from 0° to 90°, the velocity out of point A decreased from 12.1×10^{-5} to 4.26×10^{-5} m/s, and the velocity out of point B increased from 0.32×10^{-5} to 3.16×10^{-5} m/ s (Table 2). In addition, as the angle of CO₂ injection increased, more fluid exited from outlets P2 and P3, and the crude oil flooding and CO₂ storage within the porous media became more uniform. It should be mentioned that point A is in the main flow path and has a high velocity. Therefore, point A is chosen to represent the flow and composition change in the main flow channel. Point B is far away from the main flow path and has a relatively low velocity. Therefore, point B is chosen to represent the flow and composition change in the region away from main flow channel. By comparing



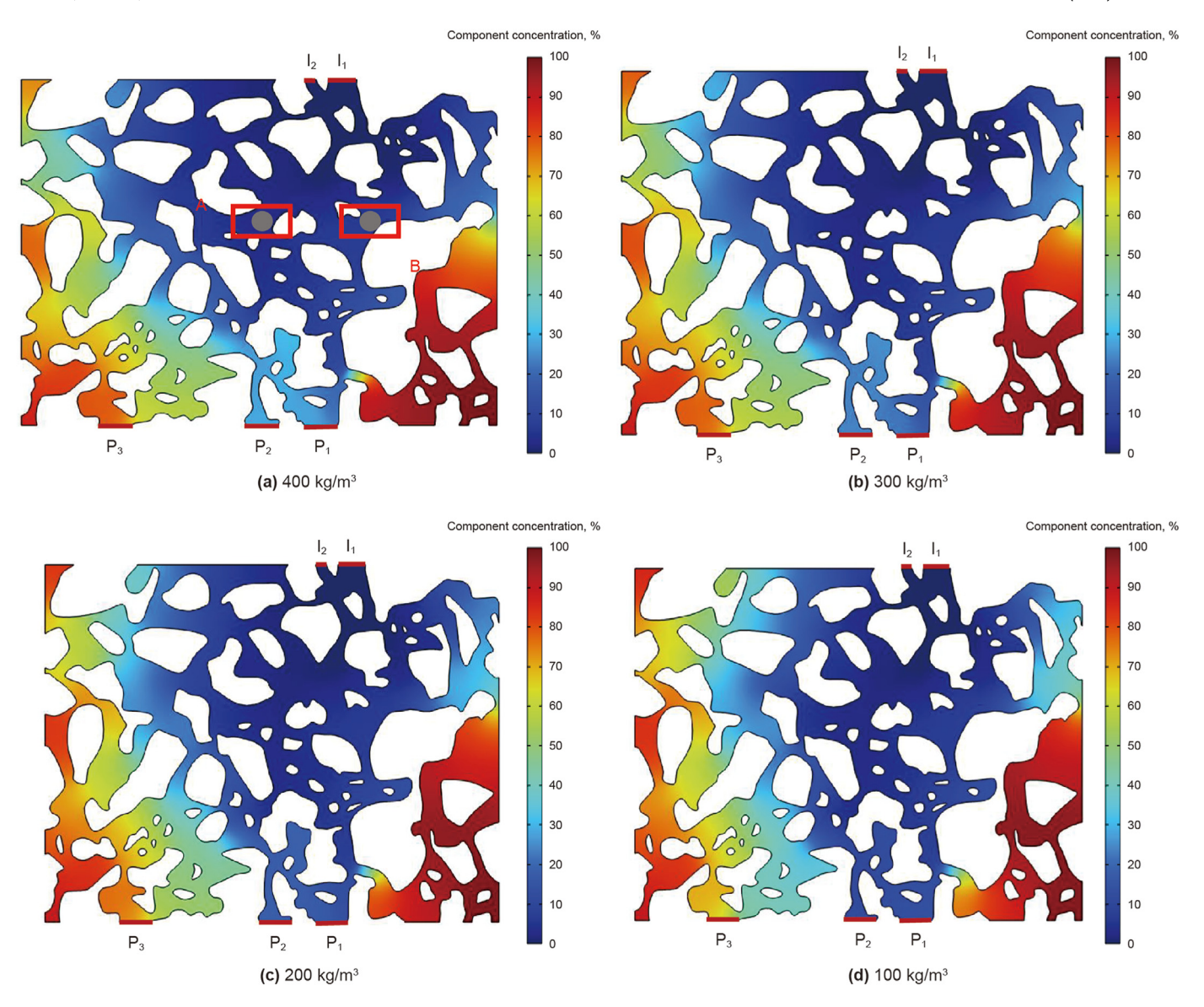
 $\textbf{Fig. 8.} \ \ \textbf{Spatial distribution of fluid velocities at different density differences after 800 s of CO_2 injection.}$

the velocity and composition difference between points A and B, the gravity-assisted effects on CO₂ flooding and storage effect can be clearly illustrated.

As the injection angle increased, the CO_2 breakthrough time was gradually delayed, and the amount of stored CO_2 increased gradually. When injected horizontally, the CO_2 breakthrough time was 216 s (Table 2), the final crude oil recovery was 59.6%, and the final CO_2 storage amount was 0.99×10^{-7} mol. When the porous medium was rotated by 90° and CO_2 was injected from the top, the CO_2 breakthrough time was delayed to 300 s, the final crude oil recovery was 82.2%, and the final amount of CO_2 storage mole was 1.37×10^{-7} mol. As the CO_2 injection angle increased from 0° to 90° , the final crude oil recovery increased by 22.6%, and the final amount of CO_2 storage mole increased by 37.9% (Fig. 6).

3.2. Density difference

Differences in pressure and crude oil composition between reservoirs resulted in significant differences in the densities of CO_2 and crude oil. Consequently, the gravity-assisted effect varied considerably among the reservoir conditions. In this subsection, we present a simulation of the CO_2 flooding and storage process under different CO_2 —oil density differences (100, 200, 300, and 400 kg/m³) and an analysis of the effect of the density differences on the gravity-assisted action. The initial and boundary conditions used in the simulations are expressed by Eqs. (5)—(17). The injection angle of 90° is chosen to simulate different density differences because the spatial distribution of fluid velocity and component concentration is the most different at 90° , which can more clearly show the influence of gravity-assisted effect on CO_2 flooding and storage.



 $\textbf{Fig. 9.} \ \ \textbf{Spatial distribution of component concentrations at different density differences after 800 s of CO_2 injection. \\$

It is also because the 90° conditions are consistent with a CO_2 flooding process in the oil reservoirs with a gas cap (Fig. 7). The CO_2 injection velocity is 6×10^{-5} m/s and the component diffusion coefficient is 5.4×10^{-9} m²/s.

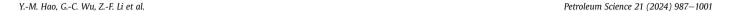
As the density difference between the CO_2 and oil increased, the difference in the spatial distribution of velocity within the porous medium decreased. Taking points A and B as examples (Fig. 8(a)), when the CO_2 —oil density difference was 100 kg/m³, the velocity at point A was 6.49×10^{-5} m/s, and the velocity at point B was 3.42×10^{-5} m/s, which is 1.90 times the velocity at point A. When the CO_2 —oil density difference was 400 kg/m³, the velocities at points A and B were 4.86×10^{-5} and 3.74×10^{-5} m/s, respectively. In this case, the velocity at point A was 1.30 times higher than that at point B. This indicates that the more significant the CO_2 —oil density difference, the more uniform the fluid flow within the porous medium. In addition, the less significant the density difference between CO_2 and oil, the higher the concentration of the remaining oil component within the porous medium after CO_2

 Table 3

 Velocity and oil component concentration at each marker point in porous media.

Density difference, kg/m ³	Velocity, 10 ⁻⁵ m/s		Oil mole fraction, %	
	Point A	Point B	Point A	Point B
100	6.49	3.42	1.80	22.10
200	5.98	3.56	2.00	18.30
300	5.38	3.67	3.20	12.60
400	4.86	3.74	3.80	7.40

injection, and the more uneven the distribution. Taking points A and B as examples (Fig. 9(a)), when the density difference between CO_2 and oil was 400 kg/m³, the molar fractions at points A and B were 3.8% and 7.4%, respectively, with a difference of 3.6%. When the density difference between CO_2 and oil was 100 kg/m³, the molar fractions at points A and B were 1.8% and 22.1%, respectively, showing a difference of 20.3% (Table 3). This is because the less significant the density difference, the higher the velocity at point A



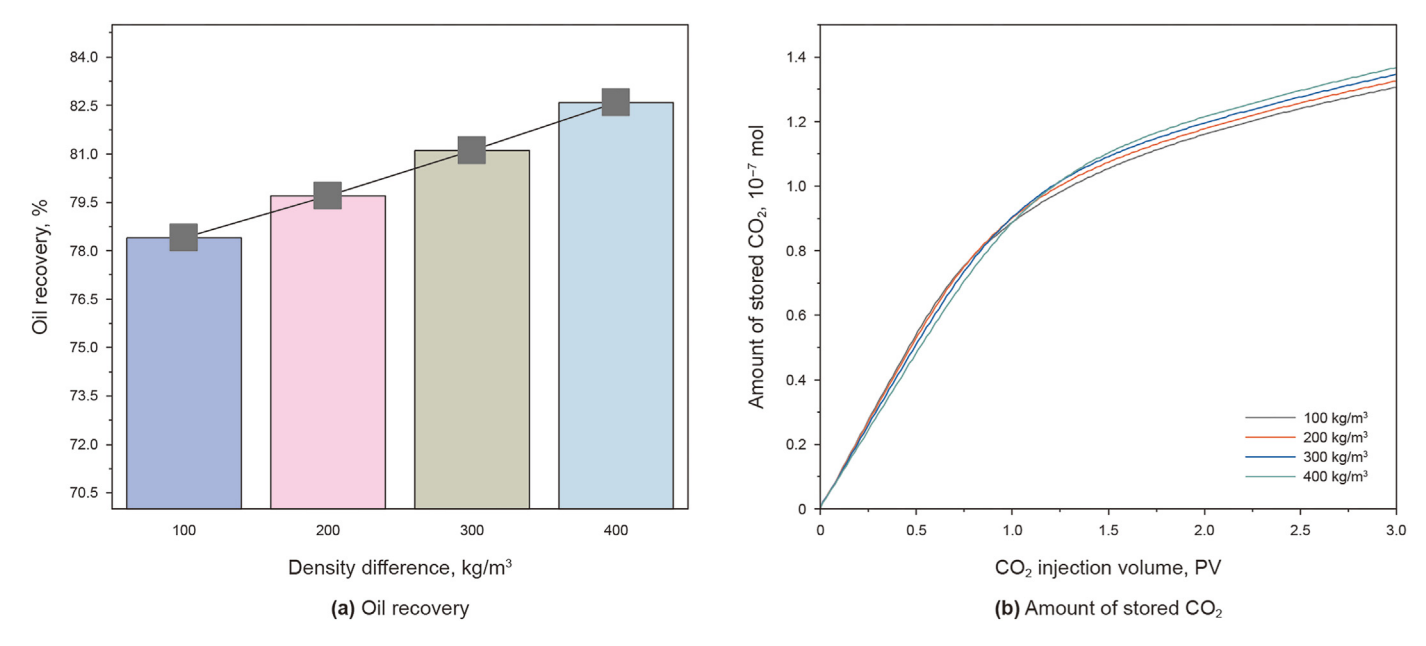


Fig. 10. Variations in oil recovery and CO2 storage amount at different density differences.

within the main channel, the more CO_2 flows through the main channel and recover the oil components, and more oil in the area around the main channel are retained within the porous medium. This suggests that the more significant the CO_2 —oil density difference, the more favorable the gravitational effect on the CO_2 flooding and storage.

As the density difference between the CO_2 and oil increased, the degree of crude oil recovery in the porous media and the CO_2 storage amount increased gradually (Fig. 10). When the density difference between CO_2 and oil increased from 100 to 400 kg/m³, the degree of recovery increased by 4.2%, and the CO_2 storage amount increased by 4.7%. Therefore, it is necessary to investigate gravity-assisted CO_2 flooding and storage in reservoirs with significant oil— CO_2 density differences.

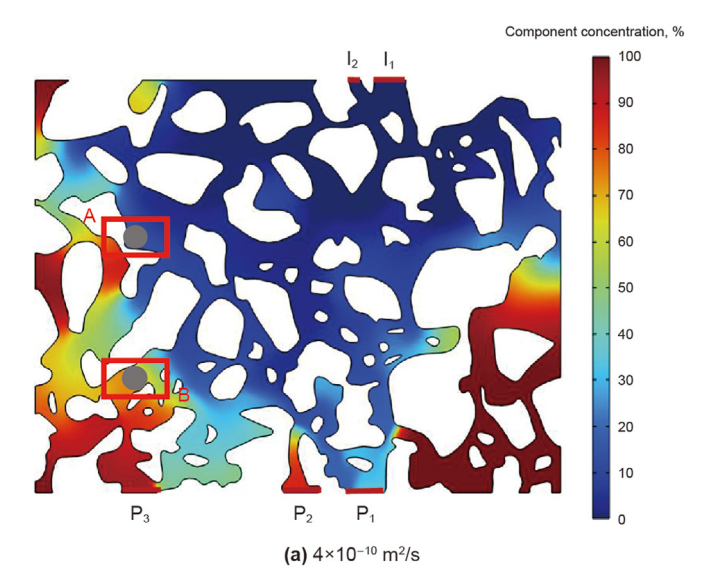
3.3. Diffusion coefficient

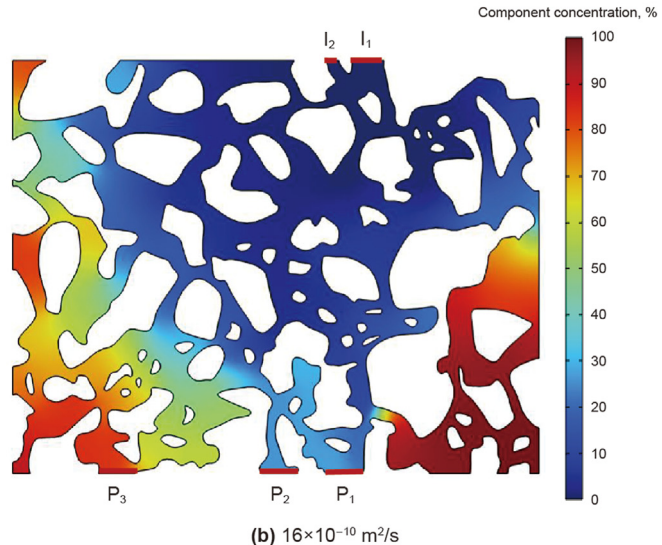
Component diffusion is a critical factor that influences CO_2 flooding and storage. In this section, we present a simulation of the CO_2 flooding and storage process at different component diffusion coefficients (ranging from 4×10^{-10} to 28×10^{-10} m²/s) and an analysis of the effect of component diffusion on CO_2 flooding and storage. Chen et al. (2022) investigated the range of diffusion coefficient values of CO_2 in crude oil in porous media, considering the effects of pressure, temperature, crude oil density, and viscosity. The diffusion coefficients reported in this subsection were selected based on the results reported by Chen et al. (2022). The initial and boundary conditions used in the simulations are expressed by Eqs. (5)–(17). The CO_2 –oil density difference is 400 kg/m³, the CO_2 injection angle is 90° , and the CO_2 injection velocity is 6×10^{-5} m/s.

As the component diffusion coefficient increased, the concentration of oil components remaining in the porous medium after CO₂ injection decreased and became more evenly distributed. This indicates that the higher the component diffusion coefficient, the more favorable it is for CO₂ flooding and storage. Taking points A

and B as examples (Fig. 11(a)), the molar fractions at points A and B were 14% and 72%, respectively, when the component diffusion coefficient was 4×10^{-10} m²/s, and the difference between the two was 58%. When the component diffusion coefficient was 28×10^{-10} m²/s, the molar fractions at points A and B were 30% and 50%, respectively, with a difference of 20%. This is because the transportation of components within a porous medium is influenced by fluid flow and component diffusion. The higher the component diffusion coefficient, the faster the CO₂ in the highvelocity flow region (point A) diffused into the low-velocity percolation region (point B) owing to the oil/CO₂ component concentration gradient. In addition, because diffusion is a two-way process, the higher the component diffusion coefficient, the faster the oil component in the low-velocity percolation region diffused into the high-velocity percolation region. Therefore, the higher the component diffusion coefficient, the higher the molar fraction of the oil components at point A, and the difference with those at point B decreases.

Under the same CO₂ injection volume conditions, the higher the component diffusion coefficient, the higher the degree of crude oil recovery from porous media, and the higher the amount of stored CO2; however, in the early stage of CO2 injection, the degree of crude oil recovery did not change significantly. When the component diffusion coefficient increased from 4×10^{-10} to 16×10^{-10} m²/s, the degree of crude oil recovery increased from 78.1% to 80.4%, with an increase of 2.3%, and the amount of stored CO_2 increased from 1.30×10^{-7} to 1.34×10^{-7} mol, with an increase of 3.1%. When the component diffusion coefficient increased from 16×10^{-10} to 28×10^{-10} m²/s, the degree of crude oil recovery increased from 80.4% to 83.8%, with an increase of 3.4%, and the amount of stored CO_2 increased from 1.34 \times 10⁻⁷ to 1.39×10^{-7} mol, showing an increase of 3.7% (Fig. 12). This indicates that component diffusion synergizes with gravity in promoting the CO₂ flooding and storage process.





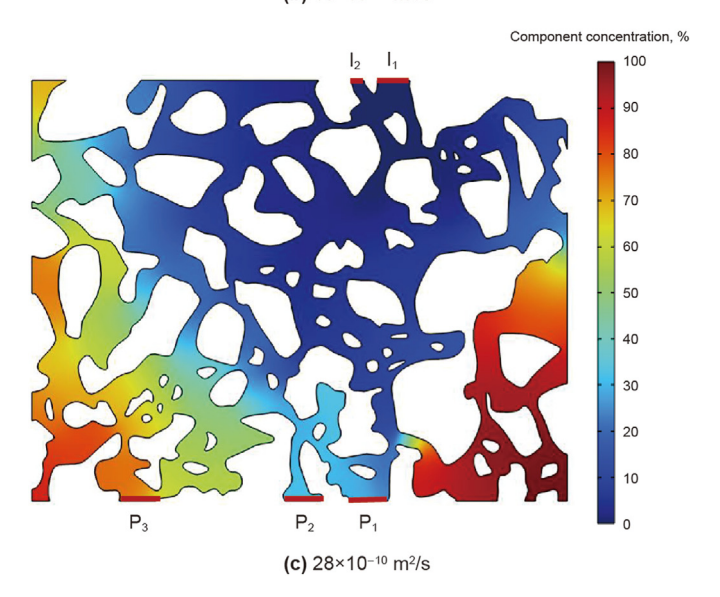


Fig. 11. Spatial distribution of component concentrations at different diffusion coefficients after 800 s of CO₂ injection.

3.4. Injection velocity

The injection velocity significantly influenced the stability and gravity-assisted effect of the CO_2 -repellent leading edge. In this study, the CO_2 flooding process was simulated at different injection velocities $(1.0\times 10^{-5}, 3.5\times 10^{-5}, \text{ and } 6.0\times 10^{-5}\,\text{m/s})$ to analyze the effect of the injection velocity on the gravity-assisted influence. The porous medium was rotated by 90° , and CO_2 was injected from the top. The initial and boundary conditions of the simulation are expressed by Eqs. (5)-(17). The $CO_2-\text{oil}$ density difference is $400\,\text{kg/m}^3$, the CO_2 injection angle is 90° , and the component diffusion coefficient is $5.4\times 10^{-9}\,\text{m}^2/\text{s}$. In the CO_2 flooding project in the actual oil reservoirs, the CO_2 leading edge moved at a velocity lower than $5.8\times 10^{-5}\,\text{m/s}$ (5 m/d). In our study, the CO_2 injection velocity is from 1.0×10^{-5} to $6.0\times 10^{-5}\,\text{m/s}$, which is close to the CO_2 leading edge movement velocity in actual oil reservoirs.

As the CO₂ injection velocity increased, the difference in the spatial distribution of velocity within the porous medium increased gradually (Table 5). Taking points A and B as an example (Fig. 13(a)), when the CO₂ injection velocity was 1.0×10^{-5} m/s, the velocities at points A and B were 4.08×10^{-6} and 3.13×10^{-6} m/s, respectively; the velocity at point A was 1.30 times that at point B. When the CO₂ injection velocity was 6.0×10^{-5} m/s, the velocity at point A was 5.83×10^{-5} m/s, and the velocity at point B was 2.96×10^{-5} m/s; the velocity at point A was 1.97 times that at point B (Table 5). This indicates that the fluid flow within the porous medium was more inhomogeneous under high-injection-velocity conditions than under low-injection-velocity conditions.

Component transport in porous media is influenced by the fluid flow and component diffusion. Under the same CO₂ injection conditions, the lower the injection velocity, the more time is available for the oil fraction in the low-velocity flow region (point E) to move via diffusion to the high-velocity percolation region (point D) and for the CO₂ in the high-velocity percolation region to move to the low-velocity percolation region (Fig. 13(d)). Consequently, the distributions of the oil and CO₂ components within the porous medium were more uniform under low-injection-velocity conditions than under high-injection-velocity conditions. The higher the diffusion coefficient, the higher the oil fraction concentration at point D, and the lower the oil fraction concentration at point E owing to diffusion (Table 4).

Because a low injection velocity facilitates uniform fluid flow within the porous medium, the lower the CO₂ injection velocity, the higher the degree of crude oil recovery within the porous medium, and the higher the amount of stored CO₂. As the CO₂ injection velocity increased from 1.0×10^{-5} to 6.0×10^{-5} m/s, the degree of crude oil recovery decreased from 91.4% to 81.9%. In addition, the amount of stored CO_2 decreased from 1.55 \times 10⁻⁷ to 1.34×10^{-7} mol, indicating a reduction of 13.5%. The higher the CO₂ injection velocity, the more significant the effect of the change in the injection velocity on the CO_2 flooding. When the injection velocity increased from 1.0 \times 10⁻⁵ to 3.5 \times 10⁻⁵ m/s, the degree of crude oil recovery in the porous medium decreased from 91.4% to 88.9% (a reduction of 2.5 %), and the amount of stored CO₂ decreased from 1.55 \times 10^{-7} to 1.48 \times 10^{-7} mol (a reduction of 4.5 %). When the injection velocity increased from 3.5×10^{-5} to 6.0×10^{-5} m/s, the degree of crude oil recovery within the porous media decreased from 88.9% to 81.9% (a decrease of 7%), and the amount of stored CO_2 decreased from 1.48 \times 10^{-7} to 1.34×10^{-7} mol (a decrease of 9.5%) (Fig. 14). Thus, a low injection velocity is beneficial for assisting gravity during CO2 miscible flooding and storage, and the gas flooding leading-edge advance



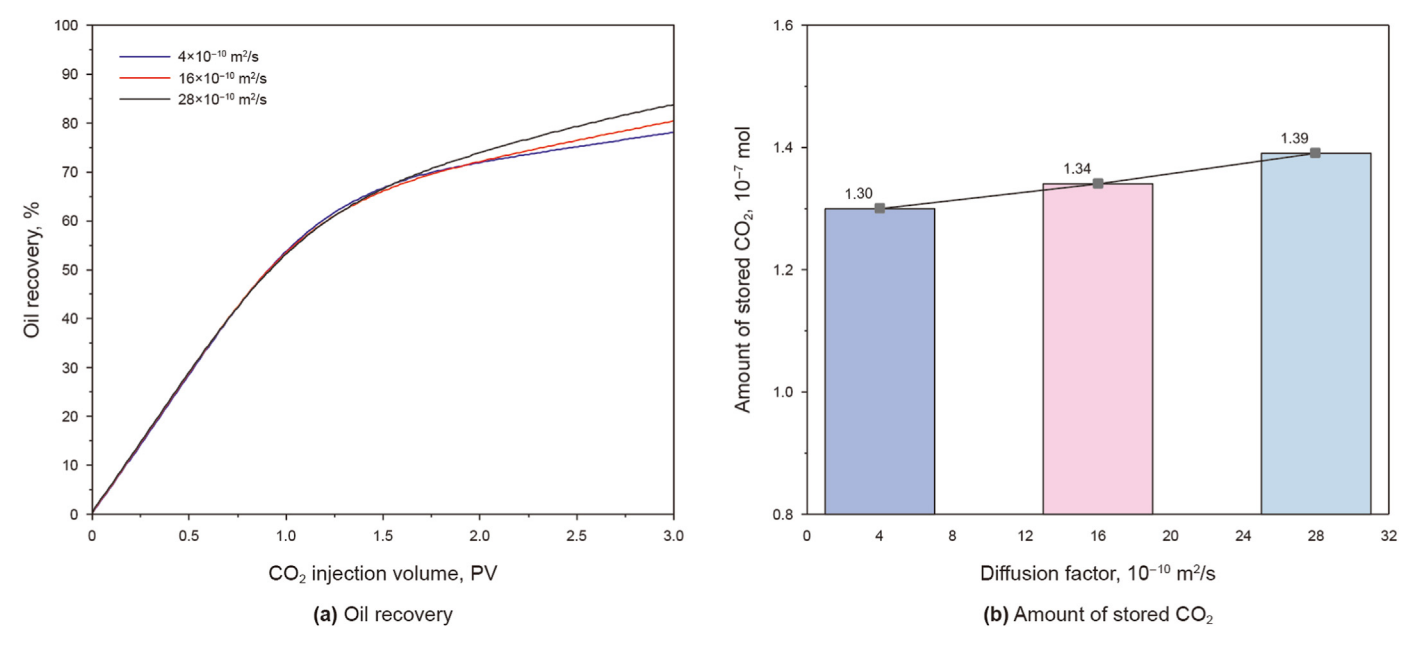


Fig. 12. Variations in oil recovery and CO2 storage amount at different component diffusion coefficients.

Table 4 Times taken for CO_2 injection at 1.5 PV and distributions of oil components at each marker point.

Injection velocity, 10 ⁻⁵ m/s	Time, s	Oil mole fraction, %		
		Point D	Point E	
1.0	4800	15.20	48.10	
3.5	1371	5.30	67.20	
6.0	800	1.50	81.50	

Table 5 Velocities at outlet in porous media.

Injection velocity, 10^{-5} m/s	Velocity, 10 ⁻⁵ m/s		
	Point A	Point B	Point C
1.0	0.41	0.31	0.30
3.5	2.11	1.30	0.66
6.0	5.83	2.96	0.85

velocity should not exceed 3.5×10^{-5} m/s.

4. Conclusions

In this study, we developed a mathematical model for pore-scale CO_2 injection in oil-saturated porous media, incorporating gravity-assisted effects. It should be noted that in field-scale oil reservoirs, in addition to gravity-assisted effects, CO_2 injection for EOR and CO_2 storage will be affected by compartmentalization, non-homogeneity, sedimentary law etc., which will be more complicated than the target of our study. Based on the simulation results,

the main conclusions of this study are as follows:

- (1) The gravity-assisted effect resulted in more uniform fluid flow in porous media, effectively delaying the CO₂ flooding breakthrough time and increasing the degree of crude oil recovery and CO₂ storage. As the CO₂ injection angle increased from 0° to 90°, the degree of crude oil recovery and CO₂ storage increased by 22.6% and 37.9%, respectively.
- (2) The larger the CO₂—oil density difference, the more favorable the gravity effect on the CO₂ flooding and storage, and the more uniform the fluid flow in porous media. As the CO₂—oil density difference increased from 100 to 400 kg/m³, the degree of crude oil recovery and CO₂ storage increased by 4.2% and 4.7%, respectively.
- (3) The higher the component diffusion coefficient, the faster the CO_2 diffusion from the high-velocity flow region to the low-velocity seepage region. This contributes to transporting the crude oil in the low-velocity flow region and achieving CO_2 storage. As the component diffusion coefficient increased from 4×10^{-10} to 28×10^{-10} m²/s, the degree of crude oil recovery and CO_2 storage increased by 5.7% and 6.9%, respectively.
- (4) The lower CO_2 injection velocity synergizes with component diffusion for more uniform fluid flow in porous media, resulting in increases of 9.5% and 15.7% in crude oil recovery and CO_2 storage, respectively. Low injection velocities can assist gravity assistance for CO_2 EOR and storage, and the advancing velocity of CO_2 front should not exceed 3.5×10^{-5} m/s (3.02 m/d).

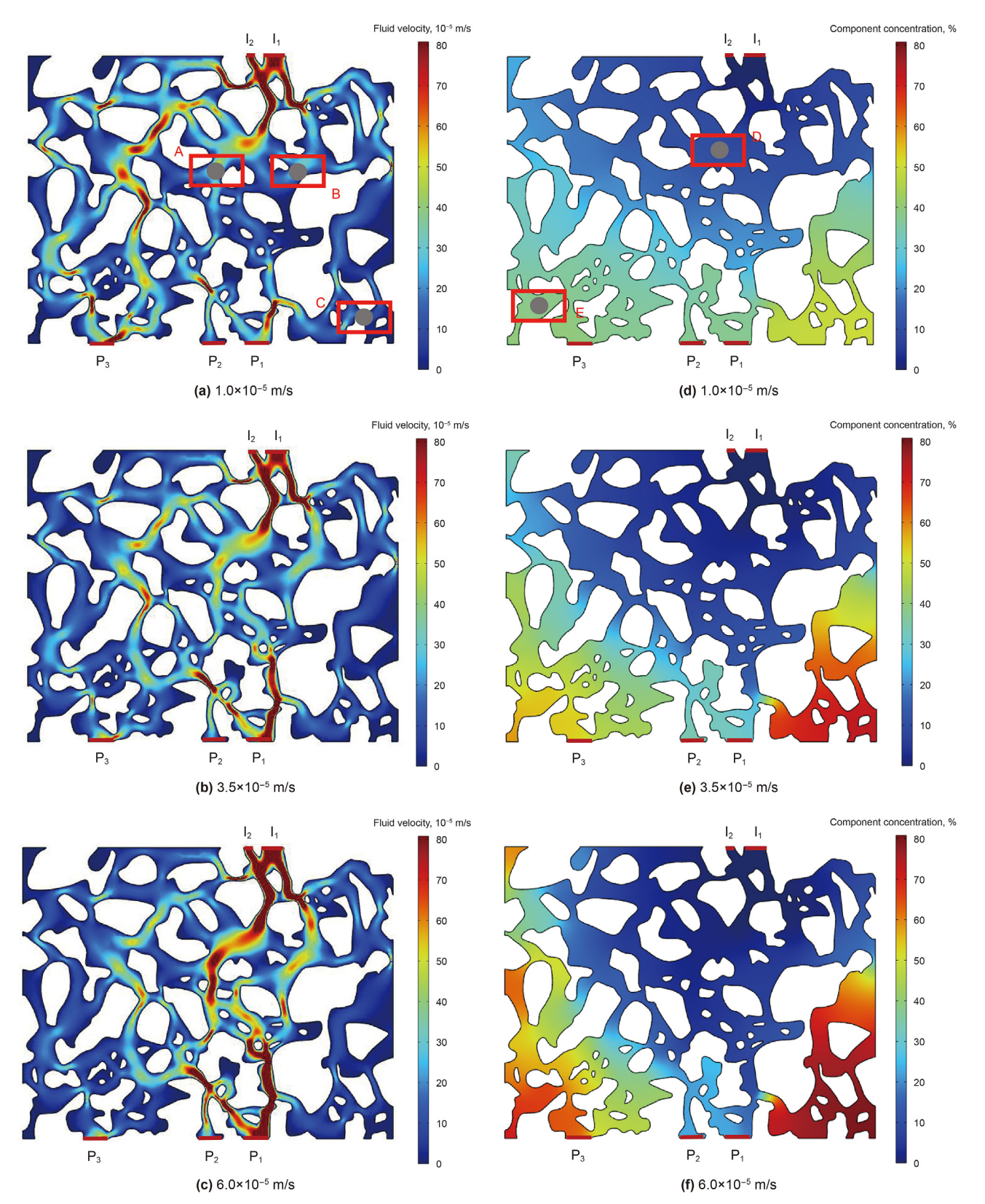


Fig. 13. Spatial distributions of fluid velocity and component concentration at different injection velocities after CO₂ injection at 1.5 PV.

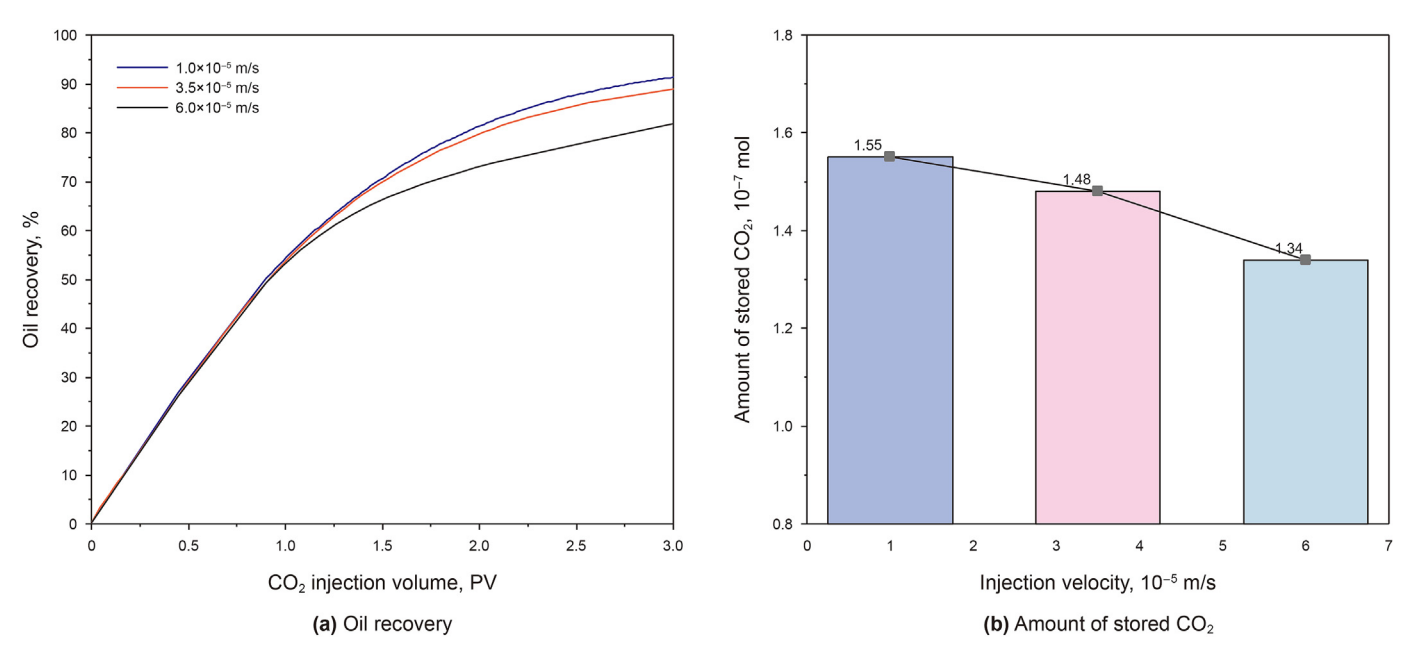


Fig. 14. Variations in oil recovery and CO₂ storage amount at different injection velocities.

CRediT authorship contribution statement

Yong-Mao Hao: Project administration, Methodology, Funding acquisition. Gui-Cheng Wu: Software, Data curation, Conceptualization. Zong-Fa Li: Visualization, Validation. Zhong-Hui Wu: Investigation. Yong-Quan Sun: Formal analysis, Conceptualization. Ran Liu: Writing — original draft. Xing-Xing Li: Writing — original draft. Bo-Xin Pang: Writing — review & editing. Nan Li: Writing — review & editing.

Declaration of competing interest

The authors declare that they have no known competing financial interests or personal relationships that could have appeared to influence the work reported in this paper.

Acknowledgements

The project supported by National Natural Science Foundation of China (No. 51991364, 51974347) and the Major Scientific and Technological Projects of CNPC under Grant ZD2019-184-002.

References

Adel, I.A., Zhang, F., Bhatnagar, N., et al., 2018. The impact of gas-assisted gravity drainage on operating pressure in a miscible CO₂ Flood. In: SPE Improved Oil Recovery Conference. https://doi.org/10.2118/190183-MS.

Beaton, M.L., Mashhadi, N., Dominato, K.R., et al., 2022. Monitoring CO₂ injection and retention in steam-assisted gravity drainage (SAGD) operations. J. Petrol. Sci. Eng. 218, 111050. https://doi.org/10.1016/j.petrol.2022.111050.

Behnoud, P., Movaghar, M.R.K., Sabooniha, E., 2023. Numerical analysis of pore-scale CO₂-EOR at near-miscible flow condition to perceive the displacement mechanism. Sci. Rep. 13 (1), 12632. https://doi.org/10.1038/s41598-023-39706-1.

Chen, H., Wang, Y., Zuo, M.S., et al., 2022. A new prediction model of CO₂ diffusion coefficient in crude oil under reservoir conditions based on BP neural network. Energy 239, 122286. https://doi.org/10.1016/j.energy.2021.122286.

Cheng, Q.G., Li, Z.X., Zhu, G.S., 2017. Research and application of CO₂ flooding to improve oil recovery in low permeability oilfield. In: 6th International Conference on Energy and Environmental Protection (ICEEP). AER-Advances in

Engineering Research, Zhuhai, China, pp. 764–768. https://doi.org/10.2991/iceep-17.2017.133.

Gong, H.J., Qin, X.J., Shang, S.X., et al., 2020. Enhanced shale oil recovery by the huff and puff method using CO₂ and cosolvent mixed fluids. Energy & Fuels 34, 1438–1446. https://doi.org/10.1021/acs.energyfuels.9b03423.

Han, J.J., Lee, M., Lee, W., et al., 2016. Effect of gravity segregation on CO₂ sequestration and oil production during CO₂ flooding. Appl. Energy 161, 85–91. https://doi.org/10.1016/j.apenergy.2015.10.021.

Huang, L.J., Li, Z.F., Ren, S.R., et al., 2021. Risk assessment and enhanced oil recovery effect of gravity assisted oxygen-reduced air flooding. In: SPE/IATMI Asia Pacific Oil & Gas Conference and Exhibition. https://doi.org/10.2118/205660-MS.

Kitao, T., Fukumoto, Y., Fujisawa, K., et al., 2021. Validation of LBM simulation of saturated seepage flow through 3D-printed homogeneous porous medium for fluid-particle coupled analysis. Acta Geotechnica 16, 2643–2656. https:// doi.org/10.1007/s11440-021-01210-z.

Kong, D.B., Lian, P.Q., Zhu, W.Y., et al., 2020. Pore-scale investigation of immiscible gas-assisted gravity drainage. Phys. Fluids 32. https://doi.org/10.1063/ 5.0033027.

Lauser, A., Hager, C., Helmig, R., et al., 2011. A new approach for phase transitions in miscible multi-phase flow in porous media. Adv. Water Resour. 34, 957–966. https://doi.org/10.1016/j.advwatres.2011.04.021.

Li, J., Cui, C.Z., Wu, Z.W., et al., 2023a. Simulation of microscopic seepage characteristics of interphase mass transfer in CO₂ miscible flooding under multiphysics field coupling conditions. ACS Omega 8 (11), 10062–10076. https://doi.org/10.1021/acsomega.2c07393.

Li, Z.F., Liu, J.H., Su, Y.L., et al., 2023b. Influences of diffusion and advection on dynamic oil-CO₂ mixing during CO₂ EOR and storage process: experi-mental study and numerical modeling at pore-scales. Energy 267, 126567. https://doi.org/10.1016/j.energy.2022.126567.

Liu, J.J., Song, R., 2015. Investigation of water and CO₂ flooding using pore-scale reconstructed model based on micro-CT images of Berea sandstone core. Prog. Comput. Fluid Dynam. Int. J. 15, 317–326. https://doi.org/10.1504/ PCFD.2015.072013.

Liu, Y.L., Rui, Z.H., 2022. A storage-driven CO₂ EOR for a net-zero emission target. Engineering 18, 79–87. https://doi.org/10.1016/j.eng.2022.02.010.

Long, Z.D., Cai, H.Z., Hu, X.Y., et al., 2020. Parallelized 3-D CSEM inversio-n with secondary field formulation and hexahedral mesh. IEEE Trans. Geosci. Rem. Sens. 58, 6812–6822. https://doi.org/10.1109/TGRS.2020.2976111.

Long, A.L., Qi, Q.S., Chen, X.L., et al., 2021. Full-Diameter physical simulat-ion of oxygen-reducing air assisted gravity drainage: a case study of Gasikule E¹₃ reservoir in Qinghai Oilfield. Xinjing Pet. Geol. 42, 565–571. https://doi.org/ 10.7657/XIPC20210508

Peng, Y.F., Li, Y.Q., Sarma, H.K., et al., 2020. Feasibility of combining gas-assisted gravity drainage (GAGD) with water injection in a thick hetero-geneous carbonate reservoir using 3-D experimental physical model and simulation. In: SPE Annual Technical Conference and Exhibition. https://doi.org/10.2118/201575-

MS

- Sepehri, E., Siavashi, M., 2022. Pore-scale direct numerical simulation of fluid dynamics, conduction and convection heat transfer in open-cell Voronoi porous foams. Int. Commun. Heat Mass Tran. 137, 106274. https://doi.org/10.1016/j.icheatmasstransfer.2022.106274.
- Song, R., Tang, Y., Wang, R., et al., 2023. Pore-scale numerical simulation of CO₂-oil two-phase flow: a multiple-parameter analysis based on phase-field method. Energies 16 (1), 82. https://doi.org/10.3390/en16010082.
- Soomro, M., Ayala, L.F., Peng, C., 2023. Fugacity-based lattice Boltzmann method for multicomponent multiphase systems. Phys. Rev. 107 (1), 015304. https:// doi.org/10.1103/PhysRevE.107.015304.
- Sun, J.M., Zhao, B., Gao, D.K., et al., 2021. Heat transfer analysis of evapora-tor of air source heat pump (ASHP) in case of frost based on chirplet finite element method. Therm. Sci. Eng. Prog. 26, 101134. https://doi.org/10.1016/ j.tsep.2021.101134.
- Sun, R.X., Pan, H.Q., Xiong, H.Y., et al., 2023. Physical-informed deep learning framework for CO₂-injected EOR compositional simulation. Eng. Appl. Artif. Intell. 126, 106742. https://doi.org/10.1016/j.engappai.2023.106742.
- Tao, L., Li, Z.M., Zhang, N., et al., 2009. CO₂ capture and for improving heavy oil recovery. In: 2009 Asia-Pacific Power and Energy Engineering Conference. https://doi.org/10.1109/APPEEC.2009.4918221.
- Wang, C., Liu, P.C., Wang, F.S., et al., 2018. Experimental study on effects of CO₂ and improving oil recovery for CO₂ assisted SAGD in super-heavy-oil reservoirs. J. Petrol. Sci. Eng. 165, 1073–1080. https://doi.org/10.1016/j.petrol.2018.02.058.
- Wang, D.Y., Fan, J.R., Xue, Z.Q., 2022a. Hydrodynamic analysis of CO₂ migration in heterogeneous rocks: conventional and microbubble CO₂ flooding experiments and pore-scale numerical simulations. Water Resour. Res. 58 (5), e2021WR031874. https://doi.org/10.1029/2021WR031874.
- Wang, H., Su, Y.L., Wang, W.D., et al., 2022b. CO₂-oil diffusion, adsorption and miscible flow in nanoporous media from pore-scale perspectives. Chem. Eng. J. 450, 137957. https://doi.org/10.1016/j.cej.2022.137957.

- Wang, S.H., Di, Y., Winterfeld, P.H., et al., 2021. Understanding the multiphysical processes in carbon dioxide enhanced-oil-recovery operations: a numerical study using a general simulation framework. SPE J. 26, 918–939. https://doi.org/10.2118/193879-PA.
- Xi, C.F., Wang, B.J., Zhao, F., et al., 2022. Oxidization characteristics and the-rmal miscible flooding of high pressure air injection in light oil reservoirs. Petrol. Explor. Dev. 49, 874–885. https://doi.org/10.1016/S1876-3804(22)60317-3.
- Yan, Z.C., Zhu, X., Wang, P., et al., 2022. The effect of gas injection velocity and pore morphology on displacement mechanisms in porous media based on CFD approach. J. Nat. Gas Sci. Eng. 101, 104558. https://doi.org/10.1016/ i.ingse.2022.104558.
- Yang, J.B., Hou, J.R., Qu, M., et al., 2020. Experimental study the flow behaviors and mechanisms of nitrogen and foam assisted nitrogen gas flooding in 2-D visualized fractured-vuggy model. J. Petrol. Sci. Eng. 194, 107501. https://doi.org/ 10.1016/j.petrol.2020.107501.
- Yang, X.F., Scheibe, T.D., Richmond, M.C., et al., 2013. Direct numerical simulation of pore-scale flow in a bead pack: comparison with magnetic resonance imaging observations. Adv. Water Resour. 54, 228–241. https://doi.org/10.1016/ i.advwatres.2013.01.009.
- Ye, X., Zhang, S.Y., 2020. A conforming discontinuous Galerkin finite element method: Part II. Int. J. Numer. Anal. Model. 17, 110–117. https://doi.org/10.48550/arXiv.1907.01397.
- Zhang, J.F., Liu, J.R., Feng, B., et al., 2020a. Fast forward modeling of the 3Dland controlled-source electromagnetic method based on model reduction. Chin. J.
- Geophys. 63, 3520–3533. https://doi.org/10.6038/cjg2020N0452 (in Chinese). Zhang, K.Q., Jia, N., Liu, L.R., 2020b. Quantitative distinction of thermodynamic soluble and miscible states. AIChE J. 66 (6), e16977. https://doi.org/10.1002/aic.16977.
- Zhang, W., 2013. Density-driven enhanced dissolution of injected CO₂ during long-term CO₂ geological storage. J. Earth Syst. Sci. 122, 1387–1397. https://doi.org/10.1007/s12040-013-0342-7.